

# Local density of state fluctuations in 2d multifractal superconductor

Mathieu Lizee,<sup>1,2</sup> Matthias Stosiek,<sup>3</sup> Christophe Brun,<sup>2</sup> Igor Burmistrov,<sup>4,5</sup> and Tristan Cren<sup>2</sup>

<sup>1</sup>*Laboratoire de Physique de l'École Normale Supérieure, ENS, Université PSL, CNRS, 3 Sorbonne Université, Université Paris Cité, 75005 Paris, France*

<sup>2</sup>*Institut des Nanosciences de Paris, Sorbonne Universités, UPMC Paris, France*

<sup>3</sup>*Physics Division, Sophia University, Chiyoda-ku, Tokyo 102-8554, Japan*

<sup>4</sup>*L. D. Landau Institute for Theoretical Physics, acad. Semenova av. 1-a, 142432 Chernogolovka, Russia*

<sup>5</sup>*Laboratory for Condensed Matter Physics, HSE University, 101000 Moscow, Russia*

The interplay of superconductivity and disorder is known to generate a wealth of new phenomena which have driven the history of superconductivity since its infancy. One of the major breakthroughs in the field is the celebrated quantum phase transition from superconductor to insulating state. Interestingly, the opposite effect has been reported several times : an increase of the superconducting critical temperature by disorder. One of the proposed mechanisms involves the peculiar structure of diffusive electronic wavefunctions whose multifractality can increase the superconducting pairing. Recent experiments in monolayer  $NbSe_2$  on graphene have reported  $T_c$  enhancement due to multifractal superconductivity but the theoretical models at our disposal fail to account for this  $T_c$  enhancement at the relevant level of disorder. In this work, we use an epitaxial monolayer of lead showing a simple band structure and homogenous structural disorder as a model system of a 2d multifractal superconductor in the weak-antilocalization regime. Then, we perform an extensive study of the emergent fluctuations of local density of states in this material and compare them with both analytical results and numerical solution of the attractive Hubbard model. We show that mesoscopic LDOS fluctuations allow to probe locally elastic and inelastic scattering in 2d weakly disordered materials in particular in the most interesting multifractal regime.

## I. INTRODUCTION

Since the seminal paper by Anderson, the field of wave localization in disordered media has developed immensely. In the metallic regime, mesoscopic fluctuations of conductance have been observed in a wealth of condensed matter systems signaling the diffusion of interacting electrons in a quenched disorder potential and are commonly referred to as the ‘weak localization’ signature. Although a similar signature of weak localization is predicted to emerge in mesoscopic fluctuations of local density of states (LDOS) in a quantum system, even if several groups have reported LDOS fluctuations and explored their spatial properties [1–3], the link with electronic diffusion in the material remains elusive.

Another major problem of condensed matter physics is the interplay of interactions and disorder. Not only are these questions at the heart of the many-body localization problem but they have also grown central in the field of disordered superconductors [4, 5]. Indeed, the pairing of weakly localized ‘multifractal’ electrons is predicted to yield a disorder-enhanced  $T_c$  compared to the clean metal case [6]. As a first experimental proof of this enhancement in  $NbSe_2$  monolayers has been reported [3], a deeper understanding of 2d diffusive superconductors in the multifractal regime is required to stimulate the development of better materials. Indeed, not only is  $NbSe_2$ /graphene a complex material challenging to tackle numerically but the type of disorder used in this study (random sulphur or silicon atom substitution) along with its own non trivial spatial structures raises significant issues. Thus, the need for an understanding of multifractal superconductivity and especially in the weak-antilocalization regime

of  $NbSe_2$  calls for new model systems.

In this study, we probe the mesoscopic fluctuations of local density of states (LDOS) in a purely two-dimensional weakly disordered metal with high resolution scanning tunneling spectroscopy. The strong spin-orbit coupling in our lead monolayer places us in the desired weak anti-localization regime. An independent measurement of the diffusion coefficient allows us to prove quantitatively that weak disorder effects on diffusive electrons controls the LDOS fluctuations close to the coherence peak. To strengthen our argument, we also compare our measurements with self-consistent solutions of the attractive Hubbard model on state of the art system size [7, 8]. We report the first measurements of LDOS correlations in weakly disordered 2d metals and demonstrate that the energy dependency of mesoscopic LDOS fluctuations allows us to extract the effective scattering rate of low energy single particle excitations. Finally, our work provides a new toolbox for the study of multifractal superconductivity in 2d systems which remain a huge challenge to the theoretical approaches.

## II. EXPERIMENTS

As model systems for the study of two-dimensional weakly disordered electronic systems, epitaxial monolayers of metals on semiconducting surfaces are exceptionally interesting. Firstly, their thickness of the order of the Fermi wavelength along with their good decoupling from the bulk makes them truly two-dimensional. Secondly, they show a wealth of phases with highly uniform and reproducible structural disorder without the need to

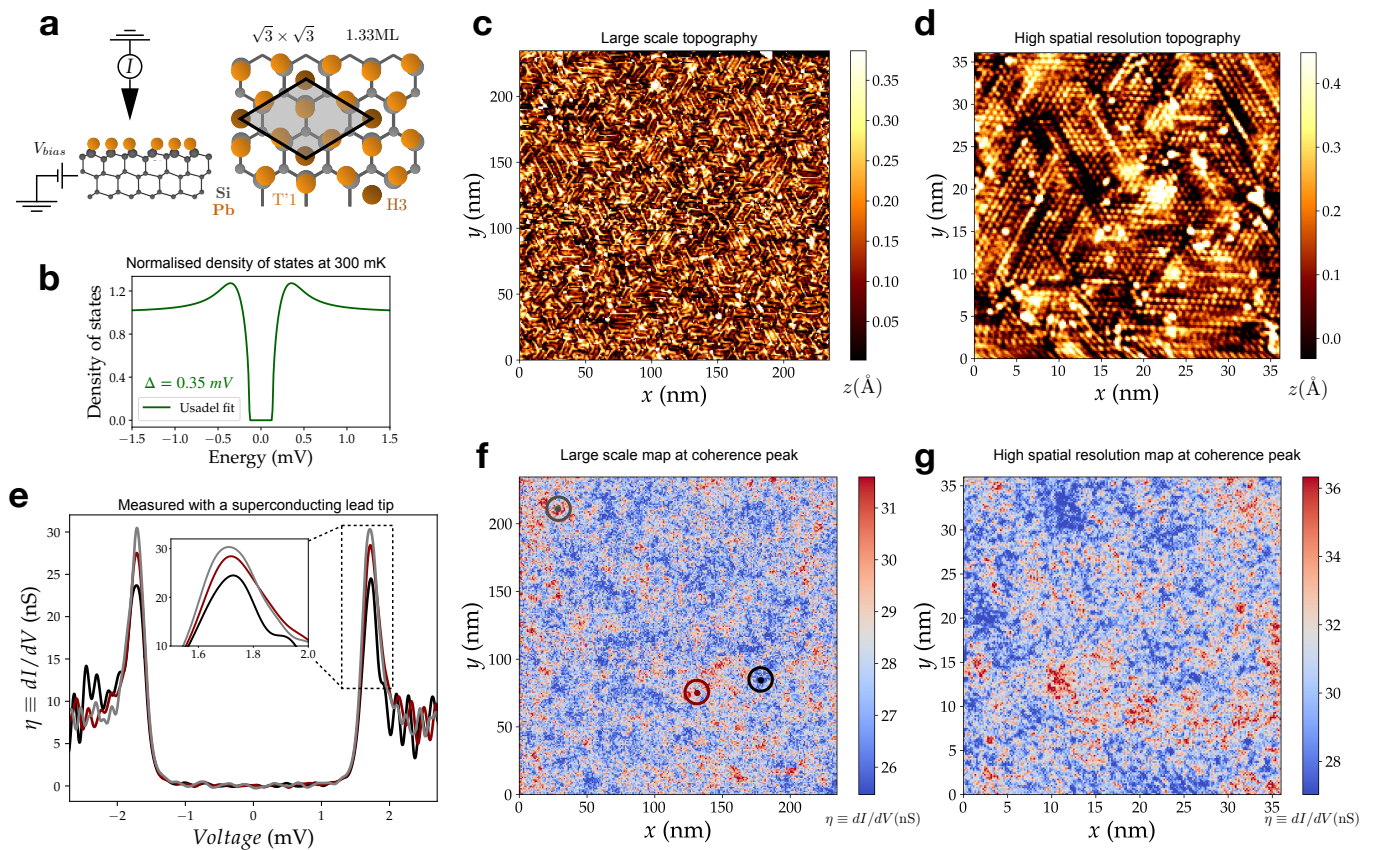


FIG. 1. **Tunneling conductance fluctuations in the SIC phase of lead on Si** **a** Description of the scanning tunneling spectroscopy measurement and of the SIC phase (1.33 ML of Pb/Si with  $\sqrt{3} \times \sqrt{3}$  symmetry). On **b**, we show the best Abrikosov-Gorkov fit of the mean density of states spectrum of the SIC phase. **c** Topographic image of the SIC monolayer phase. One clearly sees the rotational nanodomains of the  $\sqrt{3} \times \sqrt{3}$  phase separated by domain walls made of the  $\sqrt{7} \times \sqrt{3}$  reconstruction. An atomically resolved image is shown in **d**. In **e**, several differential conductance spectra ( $dI/dV$ ) measured at the positions shown on **f** are presented. On **f**, the isoenergy map corresponding to topography **c** at the coherence peak energy  $E_{max}$  is shown. Symmetrically, on **g**, we show the iso-energy  $dI/dV$  map corresponding to topography **d** at 1.7 mV.

evaporate chemical contaminants on the sample. Thus, these systems fully fabricated in ultra-high-vacuum are exceptionally clean and homogeneously disordered in contrast with the usually studied substitution alloys [1–3] where the disorder itself already has long range correlations as shown on topographic maps [2, 3]. In this work, we chose to work on the stripped incommensurate phase of lead on silicon. The ideal SIC monolayer described in Figure 1a is made of 1.33 monolayer of lead atoms on top of a Si(111) surface. The lead is evaporated on the  $7 \times 7$  reconstruction of silicon in-situ a home made scanning tunneling microscope. The SIC phase is made of nanometric domains oriented preferentially along 3 directions as shown on large scale in Figure 1c and with atomic resolution in Figure 1d. The sample is then cooled to 300 mK, well below its critical temperature of 1.8 K. On panel **b**, we show the density of states of the SIC phase in the superconducting state. In order to probe the mesoscopic fluctuations of this phase, we acquire a large scale (250 nm x 250 nm) spectroscopic map with nanometric spatial resolution. A superconducting tip (bulk lead)

is used to increase the energy resolution of the spectra. The  $dI/dV$  spectrum (Fig. 1 e) shows sharp coherence peaks at  $E_{max} = \Delta_{tip} + \Delta_{SIC} = 1.7 \text{ mV}$  in agreement with the known gap of the SIC phase  $\Delta_{SIC} \sim 0.35 \text{ mV}$ . Three individual spectra whose positions are shown in **f** are displayed in **e**. These spectra demonstrate that conductance fluctuations are stronger at the coherence peak and do not indicate large variations of the peak’s position  $E_{max}$  or in other words the gap width  $\Delta$ . Displaying the local differential conductance at a given bias voltage  $V_{bias}$  yields iso-energy  $dI/dV$  maps. On Figure 1f, we show the  $dI/dV$  map measured at the energy of the coherence peak (1.7 mV) and evidence spatial fluctuations of the differential conductance at various scales. An interesting feature of this map is indeed that no characteristic scale of the domains can be easily identified. This fractal-like property points towards non trivial origins of these mesoscopic fluctuations. Considering the nanometric scale structure of the monolayer, we also acquire a high spatial resolution spectroscopic map of 35 nm in order to better capture small scale fluctuations. On

Figure 1d and g, we show respectively the topographic and spectroscopic high spatial resolution map at 1.7 mV. Here again, the tunneling conductance shows strong spatial fluctuations at scales smaller than the superconducting coherence length which is known to be of the order of 50 nm. Finally, we show that the exquisite spatial and spectral resolution of our experiment allows us to probe tunneling conductance fluctuations on scales ranging from the Fermi wavelength  $\lambda_F$  up to several times the superconducting coherence length  $\xi \sim 50$  nm with a spectral resolution of the order of  $30 \mu\text{V}$ . [9, 10].

### III. FLUCTUATION ANALYSIS

We start our analysis by the simplest possible measure of fluctuations: the variance of iso-energy tunneling conductance maps,  $\sigma_\eta = \langle \delta\eta(V)^2 \rangle_r$  where to keep notations light, we use  $\eta$  to denote the experimentally measured differential conductance  $dI/dV$ . On Figure 2a, we plot (in green) the variance  $\langle \delta\eta^2 \rangle$  as a function of bias voltage. We obtain a characteristic curve showing a peak at the coherence peak energy  $E_{\text{max}}=1.7$  mV in agreement with the qualitative observation we make on the high resolution maps shown on Figure 2f that fluctuations are higher at the coherence peak, close to at  $V_{\text{bias}} \sim 1.7$  mV.

We now attempt to rationalise the tunneling conductance spatial fluctuations. Considering a simplified expression for the tunneling current, we write it as a zero temperature convolution of tip and sample density of states:

$$I = |t|^2 \int dE \rho_{\text{tip}}(E - eV) \rho(E) \quad (1)$$

Experimentally, the tip's height above the sample and thus the transmission's coefficient  $t$  is not constant but rather controlled by fixing the high voltage current  $I(V_\Lambda = 3 \text{ mV})$  to 2 nA. The observable we measure is therefore  $\eta$  defined as:

$$\eta(V, \mathbf{r}) = \frac{\overline{I(V_\Lambda)}}{I(V_\Lambda, \mathbf{r})} \frac{\partial I}{\partial V}(V, \mathbf{r}) \quad (2)$$

where the current  $I$  follows equation (1). From these two formulae, it is clear that density of states fluctua-

tions lead to fluctuations of tunneling conductance  $\eta$  but also that the energy dependency of these fluctuations will strongly depend on the tip density of states and the tip's control voltage  $V_\Lambda$ . However, it is also apparent that the only source of spatial fluctuations in Eq. (2) is the sample's density of states. We will therefore attempt to compare quantitatively the expected  $dI/dV$  fluctuations for a 2D disordered superconductor to the experimental measurements.

We now compute the fluctuations of density of states in a two-dimensional diffusive superconductor. These fluctuations, as the counterpart in STM measurement of the universal conductance fluctuations measured in transport experiments and are expected to scale at low disorder as  $\langle \delta\rho^2 \rangle / \langle \rho \rangle^2 \sim 1/g$ . In the following, we sketch a simplified derivation of the density of state correlator in diffusive superconductors. We have  $\rho(E, r) = -\frac{1}{\pi} \text{Im} G^R(E, r, r)$  with  $G^R(E, r, r) = \langle r | \frac{1}{E - H + i\eta} | r \rangle$ . Like in the mean-field solution to the BCS Hamiltonian, we introduce the Bogoliubov operators and coherence factors  $u_\alpha$  and  $v_\alpha$  associated to the single particle eigenstates  $\phi_\alpha$  for the eigenvalue  $\epsilon_\alpha$ . The LDOS can be written conveniently as:

$$\rho(E, r) = \sum_{a, s=\pm} \phi_a^2(r) (1 + \epsilon_a/E) \delta(E - s\sqrt{\epsilon_a^2 + \Delta^2}) \quad (3)$$

The density of states correlations are then computed from this expression along with the dynamical structure factor which is a spatially averaged product of wavefunctions measured at position  $\mathbf{r}$  and  $\mathbf{r}'$  and at well determined energies. If one neglects the dependency of single particle density of states on energy, this structure factor can be computed from the polarization operator  $\Pi^R(\omega, \mathbf{r}, \mathbf{r}')$

$$F(\epsilon, \omega, \mathbf{r}, \mathbf{r}') = \frac{1}{\pi\omega} \text{Im} \Pi^R(\omega, \mathbf{r}, \mathbf{r}') \quad (4)$$

In the diffusive regime at weak disorder, one gets for the Fourier transform of the polarization operator

$$\Pi^R(\omega, \mathbf{q}) = \rho_0 \frac{Dq^2}{Dq^2 - i\omega}, \quad (5)$$

where  $D$  denotes the diffusion coefficient and  $\rho_0$  the low energy density of states of the non interacting problem. The full derivation yields the pair LDoS correlation function at different points  $(r_1, r_2)$  and different energies  $(E_1, E_2)$ :

$$\begin{aligned} \langle \delta\rho(E_1, \mathbf{r}_1) \delta\rho(E_2, \mathbf{r}_2) \rangle = & \frac{\rho_0^2}{2\pi g} \Re \left\{ \left[ 1 + X_{E_1} X_{E_2}^* \right] K_0 \left( R \sqrt{\frac{2\gamma_\Phi - iE_1/X_{E_1} + iE_2/X_{E_2}^*}{D}} \right) \right. \\ & \left. - \left[ 1 - X_{E_1} X_{E_2} \right] K_0 \left( R \sqrt{\frac{2\gamma_\Phi - iE_1/X_{E_1} - iE_2/X_{E_2}}{D}} \right) \right\} \quad (6) \end{aligned}$$

where  $R = |\mathbf{r}_1 - \mathbf{r}_2|$ ,  $K_0$  stands for the modified Bessel

function, and  $\rho_0$  is the high energy mean density of states.

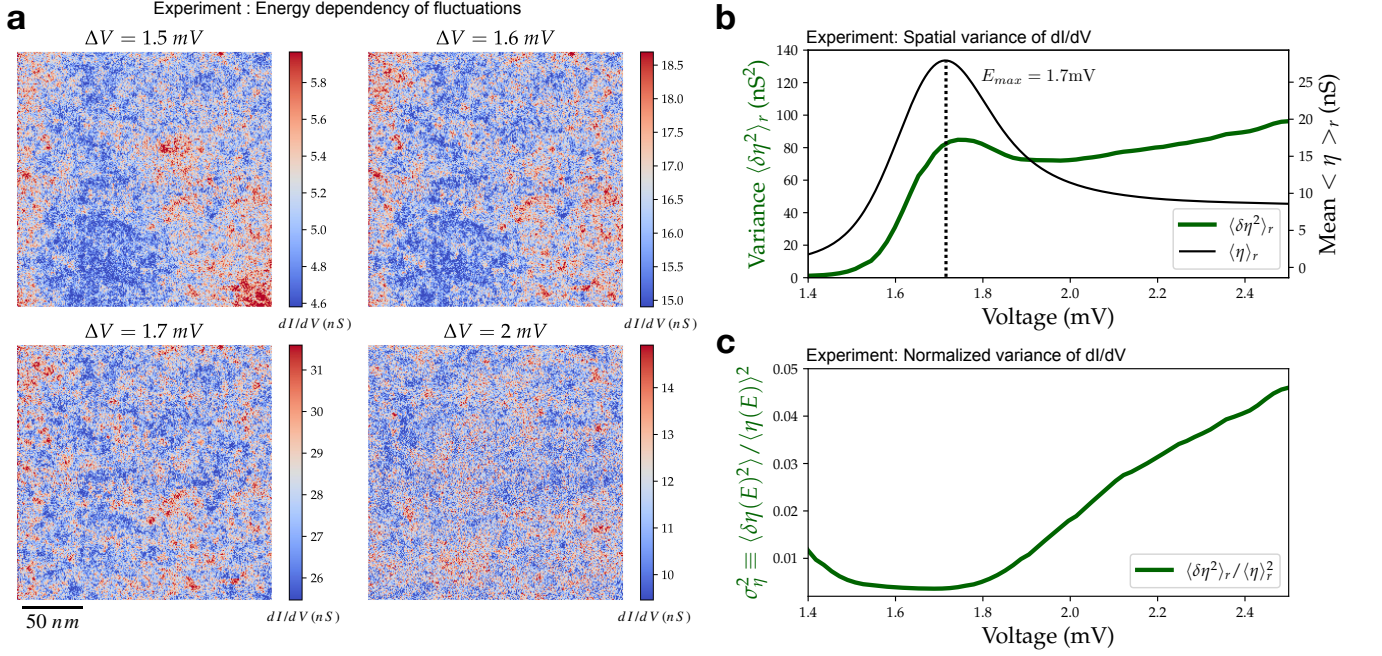


FIG. 2. **Analysis of tunneling conductance fluctuations** **a** Variance (green) and mean value (black) of the tunneling conductance  $dI/dV$  computed on iso-energy maps as a function of the bias voltage. On panels **b-e**, we describe the fluctuations of density of states computed semi-analytically as a function of energy  $E$ , conductance  $g$  and effective dephasing rate  $\gamma_\Phi$ . On **b**, we show the energy dependency of the normalized variance  $\sigma_\rho^2$  (red) at a conductance  $g=10$  and several values of  $\gamma_\Phi$ . In black, we show the mean density of states used for the calculation (see SI). On **c-e**, we now fix the energy at  $E = 2\Delta \sim 0.6$  mV and plot on **c** a color-map the log of  $\sigma_\rho^2$  as a function of both conductance and dephasing rate. On **d**, we show the dependency of  $\sigma_\rho^2$  on conductance for  $\gamma_\Phi \in [0.03, 0.25, 0.5]$  mV. On **e**, we show the dependency on dephasing rate for  $g \in [10, 20, 30]$ . On **f**, we show several conductance maps taken at  $E \in [1.7, 2, 2.5, 2.8]$  mV where we recall that  $E_{\max} = 1.7$  mV is the coherence peak energy (shifted by comparison with the sample's density of states peak  $\Delta \sim 0.3$  mV because of the superconducting tip). On **g**, we compare the experimentally measured normalized variance of tunneling conductance  $\sigma_\eta^2$  with the one computed semi-analytically from density of states correlations (Eq. 6). We plot the theoretical prediction for  $g \in [10, 20, 30, 50]$  and the levels of dephasing which best reproduce the experimental data in each case. We stress that no free parameter is used here. More details on the calculation of  $\sigma_\eta^2$  are given in SI.

Also we introduce  $X_E = E/\sqrt{E^2 - \Delta_E^2}$  where we phenomenologically substitute  $\Delta$  by the complex energy dependent gap-function  $\Delta_E$ .

Finally, two parameters control the strength of density of state fluctuations: the dimensionless conductivity  $g = hD\rho_0/2$  and the effective dephasing rate  $\gamma_\Phi$ , assumed to be energy independent in this calculation. On Figure 2**b**, we show the energy dependency of  $\sigma_\rho^2$  for a conductance fixed at  $g = 10$  and several values of  $\gamma_\Phi$  ranging typically between  $\Gamma \sim k_B T \sim 30 \mu\text{V}$  and  $\Delta \sim 250 \mu\text{V}$ . We show that  $\sigma_\rho^2$  has a local minimum at the coherence peak energy  $E_{\max}$ . On panels **c** and **d**, we show that at fixed energy,  $\sigma_\rho^2$  decreases with increasing conductivity (as expected from the  $1/g$  dependency in equation (6)). On panels **c** and **e**, we show that increasing dephasing rate  $\gamma_\Phi$  corresponding to smaller system size in a transport experiment decreases the variance  $\sigma_\rho^2$ . We stress that these dependencies are very much expected from the understanding of mesoscopic fluctuations. The larger the coherence length and low conductivity lead to enhanced fluctuations, whether one measures conduc-

tance or LDOS fluctuations.

To assess the conductance of the SIC phase and relate it to the tunneling conductance mesoscopic fluctuations, we refer to previous work where the proximity effect between two superconductors was used to estimate the diffusion coefficient of the monolayer [9]. These results are strengthened by another measurement from our group where the spatial profile of a vortex core allowed us to extract the dirty coherence length and thus the electronic diffusion coefficient [10]. Both these measurements yield a dirty coherence length  $\xi \in [45, 50]$  nm. Writing  $\xi = \sqrt{hD/\Delta}$  with  $\Delta = 0.23$  meV gives a diffusion coefficient  $D \in [7, 10]$  cm<sup>2</sup>/s. We now consider the Einstein relation for the conductivity (per spin orientation) of the monolayer  $g = hD\rho_0/2$  and write the density of states of a two-dimensional electron gas  $\rho_0 = 2 \frac{k_F}{h v_F} = \frac{2m}{2\pi\hbar^2}$  (factor of 2 for the two spin orientations). This leaves us with  $g = \frac{mD}{\hbar}$ . Using the known effective mass  $m = 1.27 m_e$  in the SIC phase [11], we can estimate  $g \in [8, 12]$ . Using equations (1) and (2), we now compute the tunneling conductance normalized variance  $\sigma_\eta^2$  for  $g$  of the order of

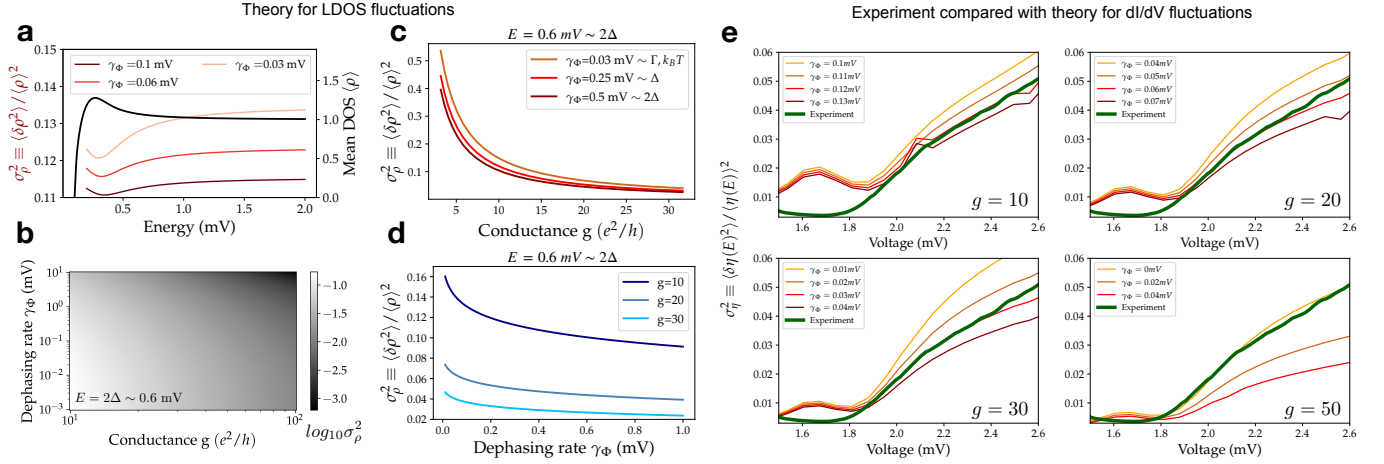


**FIG. 3. Analysis of tunneling conductance fluctuations** On panels **a-d**, we describe the fluctuations of density of states computed semi-analytically as a function of energy  $E$ , conductance  $g$  and effective dephasing rate  $\gamma_\Phi$ . On **a**, we show the energy dependency of the normalized variance  $\sigma_\rho^2$  (red) a conductance  $g=10$  and several values of  $\gamma_\Phi$ . In black, we show the mean density of states used for the calculation (see SI). On **b-d**, we now fix the energy at  $E = 2\Delta \sim 0.6$  mV and plot on **b** a color-map the log of  $\sigma_\rho^2$  as a function of both conductance and dephasing rate. On **c**, we show the dependency of  $\sigma_\rho^2$  on conductance for  $\gamma_\Phi \in [0.03, 0.25, 0.5]$  mV. On **d**, we show the dependency on dephasing rate for  $g \in [10, 20, 30]$ . On **e**, we compare the experimentally measured normalized variance of tunneling conductance  $\sigma_\eta^2$  with the one computed semi-analytically from density of states correlations (Eq. 6). We plot the theoretical prediction for  $g \in [10, 20, 30, 50]$  and the levels of dephasing which best reproduce the experimental data in each case. We stress that no free parameter is used here. More details on the calculation of  $\sigma_\eta^2$  are given in SI.

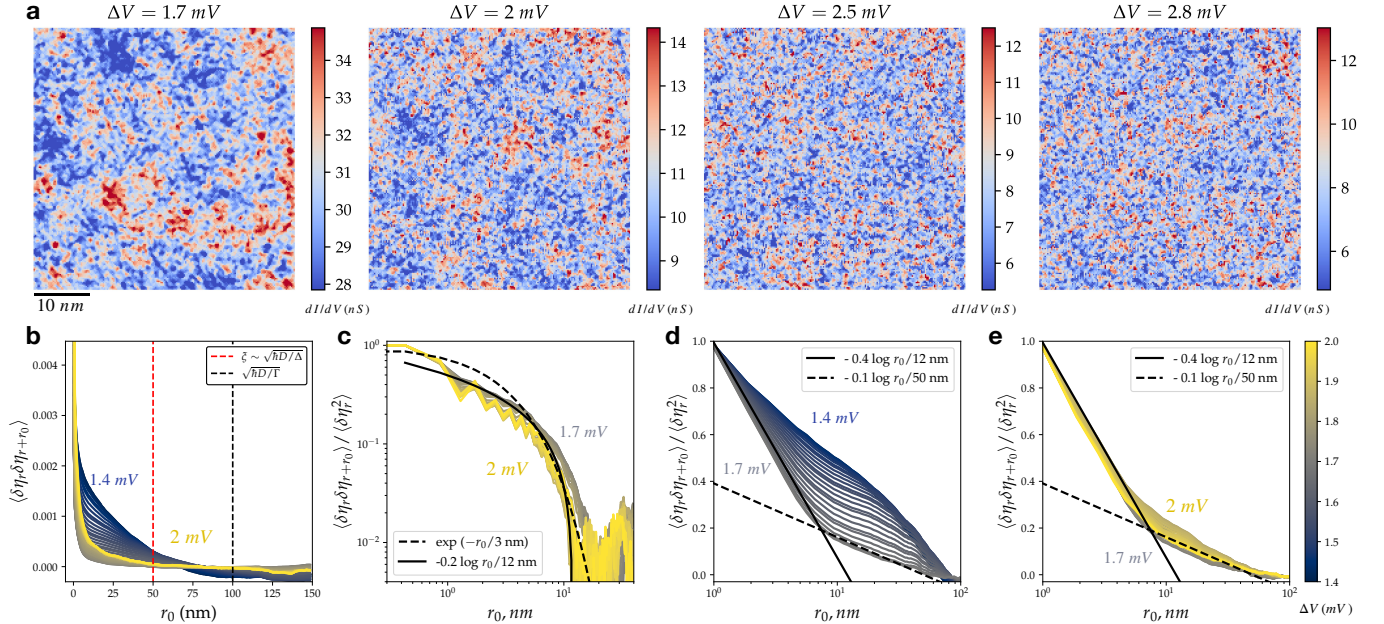


**FIG. 4.  $dI/dV$  spatial correlations** On **a**, we show several iso-energy short scale  $dI/dV$  maps for  $E \in [1.7, 2, 2.5, 2.8]$  mV. Here again, we recall that  $E_{\max} = 1.7$  mV is the energy of the coherence peak. On panel **b**, we show the angle averaged 2-point correlations on large scale maps as a function of distance and bias voltage (color scale for panels **b-e** given on panel **e**). On this plot, we also show the position of superconducting coherence length  $\xi$  (red) and the diffusion length corresponding to energy scale  $\Gamma \sim 80$   $\mu$ V (black). On **c**, we plot the angle averaged auto-correlation computed on small scale maps. On **d,e**, we use lin-log scales to evidence the peculiar behavior of the auto-correlation (normalized by its zero distance value). On **d**, we focus on energies below  $E_{\max}$  and on **e**, on energies above  $E_{\max}$ .

10 :  $g \in [10, 20, 30, 50]$ . The complete formula is given in supplementary materials and involves integration over energies of the density of states correlator given in equation (6). This calculation also involves the tip density of states (see SI Figure S1). The tunneling conductance variance  $\sigma_\eta^2$  can now be compared to experimental measurement. On Figure 2g, we plot in green the measured normalized variance  $\sigma_{\text{exp}}^2(V) = \langle \delta\eta(V)^2 \rangle_r / \langle \eta(V)^2 \rangle_r$ . The thin lines are semi-analytical calculations of  $dI/dV$  normalized variance computed for  $g \in [10, 20, 30, 50]$ . For each value of the conductance, we plot the theoretical curve for dephasing rates  $\gamma_\Phi$  which best reproduce the experimental variance. We see that in each case, the high energy part of the curve is in very good agreement between experiment and theory. We stress that no free parameter is used here as the dephasing rate  $\gamma_\Phi$  is constrained in a rather narrow window of physically relevant energies  $\gamma_\Phi \in [k_B T, \Delta] \sim [30 - 300] \mu\text{V}$ . We also emphasize that the variance at  $E_{\text{max}} = 1.7 \text{ mV}$  close to the coherence peak is rather well reproduced for  $g=10$  which is the expected conductance of the monolayer [9, 10]. While, experiment yields  $\sigma_{\text{exp}}(1.7 \text{ mV}) \sim 3.10^{-3}$ , theory for  $g = 10$  gives  $\sigma_\eta(1.7 \text{ mV}) \sim 15.10^{-3}$ . However, it is apparent on the lower panels of Figure 2g that higher conductance and lower dephasing rate yield a better agreement with experiment.

After considering the variance of the iso-energy maps and thus disregarding the spatial structure of fluctuations, we have focused on the spatial correlations of the conductance fluctuations:  $\langle \delta\eta_r \delta\eta_{r+r_0} \rangle_r$ . On Figure 3 a, we show several conductance maps at various energies where a change of regime at  $E_{\text{max}}$  is obvious. We show that spatial structures below the coherence peak are more extended than above  $E_{\text{max}}$ . Moreover, we draw the reader's attention to the peculiar nature of density of state fluctuations at  $E_{\text{max}} = 1.7 \text{ mV}$  : at this energy, no correlation length is emerging while many spatial scales are present altogether. These non-trivial statistics hints at the multifractal properties of the weakly disordered 2d-metals. To explore the iso-energy spatial correlations of tunneling conductance, we plot on b the angle-averaged 2-point correlation function as a function of distance  $r_0$ . The color of the curve represents the energy at which it is measured. On c, we use a log-log representation of the auto-correlation function (normalized by its value at 1 nm). To better show the angle averaged radial decay at various energies, we normalize this auto-correlation by its value at  $r_0 = 2 \text{ nm}$  and plot them for energies below  $E_{\text{max}}$  on Figure 3d and above  $E_{\text{max}}$  on Figure 3e where the curve's color is coding its energy below 1.4 and 2 mV. It is apparent here that above  $E_{\text{max}}$ , these auto-correlation profiles depend only very weakly on energy. On e, we show that the spatial auto-correlation has a short range regime with steep decay up to approximately 10 nm followed by a long range regime with a slower decay. As made visible with the black lines, two apparently log-decay regimes are identified with respective slopes of -0.55 and -0.15 for the short and long

range regimes respectively.

#### IV. NUMERICAL STUDY OF LDOS FLUCTUATIONS WITH THE ATTRACTIVE HUBBARD MODEL

We consider the attractive- $U$  Hubbard model on the square lattice in two-dimensions with double-periodic boundary conditions. Within the mean-field approximation the Hamiltonian reads ( $U > 0$ )

$$\hat{H} = -t \sum_{\langle i,j \rangle, \sigma} \hat{c}_{i,\sigma}^\dagger \hat{c}_{j,\sigma} + \sum_{i,\sigma} (V_i - \mu - U n(\mathbf{r}_i)/2) \hat{n}_{i,\sigma} + \sum_i \Delta(\mathbf{r}_i) \hat{c}_{i,\uparrow} \hat{c}_{i,\downarrow} + \text{h.c.} \quad (7)$$

Here  $\hat{c}_{j,\sigma}^\dagger$  and  $\hat{c}_{j,\sigma}$  stand for the creation and annihilation operators of a fermion with spin projection  $\sigma = \pm 1/2$  at a site  $j$ . An on-site random potential is drawn from the box distribution,  $V_i \in [-W, W]$ . The chemical potential  $\mu$  fixes the filling factor to 0.3; throughout this work the interaction is taken as  $U = 2.2t$ . The local occupation number  $n(\mathbf{r}_i)$  and the pairing amplitude  $\Delta(\mathbf{r}_i)$  are determined self-consistently,

$$n(\mathbf{r}_i) = \sum_\sigma \langle \hat{n}_{i,\sigma} \rangle, \quad \Delta(\mathbf{r}_i) = U \langle \hat{c}_{i,\downarrow}^\dagger \hat{c}_{i,\uparrow}^\dagger \rangle, \quad (8)$$

where  $\hat{n}_{i,\sigma} = \hat{c}_{i,\sigma}^\dagger \hat{c}_{i,\sigma}$  and the average is taken with respect to the equilibrium density matrix corresponding to the Hamiltonian (7) at zero temperature. We solve Eqs. (7)–(8) iteratively and terminate the self-consistency cycle when  $\alpha^{(n)}$ , the relative change in  $\Delta(\mathbf{r}_i)$  in iteration  $n$ , is at each site  $\mathbf{r}_i$  smaller than some  $\alpha$ :

$$\alpha^{(n)} = \max_{\mathbf{r}_i} \left| \frac{\Delta^{(n)}(\mathbf{r}_i) - \Delta^{(n-1)}(\mathbf{r}_i)}{\Delta^{(n-1)}(\mathbf{r}_i)} \right| < \alpha. \quad (9)$$

For system size  $L = 192$  we chose  $\alpha = 10^{-3}$ . We employ the Kernel Polynomial Method to compute  $n(\mathbf{r}_i)$ ,  $\Delta(\mathbf{r}_i)$  and the density of states. The underlying expansion of the time-evolution operator in Chebyshev polynomials to order  $N_C$  causes Gibbs oscillations that we deal with employing the Jackson kernel, see Ref. [7] for further computational details. The ensemble averaging over observables involves, typically, more than a hundred samples.

On Figure 5, we show the results of the numerical investigation and compare them with both the analytical theory derived earlier and the experimental results. On panels a, b, we show local density of state maps taken at  $E = E_{\text{max}}$  and  $E = 3 E_{\text{max}}$ . Like shown previously on Figure 4 for the experimental results, a strong qualitative difference is observed on the maps. Fluctuations show longer range correlations close to  $E_{\text{max}}$  than at higher energy. Then on panel c, we plot the distribution of the local density of state at fixed energy along with the corresponding

gaussian fit. Deviations from the gaussian behavior are apparent and stronger for the map at  $3 E_{\max}$ . On **d**, we compare the RMS deviation of the distribution to either a gaussian (like shown on **c**) or a log-normal model. It is clear that the log-normal model gives a more accurate description of the distribution. On panel **e**, we show the mean density of states of the numerical model (black line) along with the normalized variance  $\sigma^2$  (red). In the inset, we show a fit to the analytical formula for density of state variance. The Hamiltonian we study here features no electronic dephasing and  $\gamma_{\Phi}$  should therefore be of the order of the diffusive energy corresponding to the system size (very small). We show that several values of  $(g, \gamma_{\Phi})$  with  $g \in [50, 60, 70]$  allow to reproduce very decently the data.

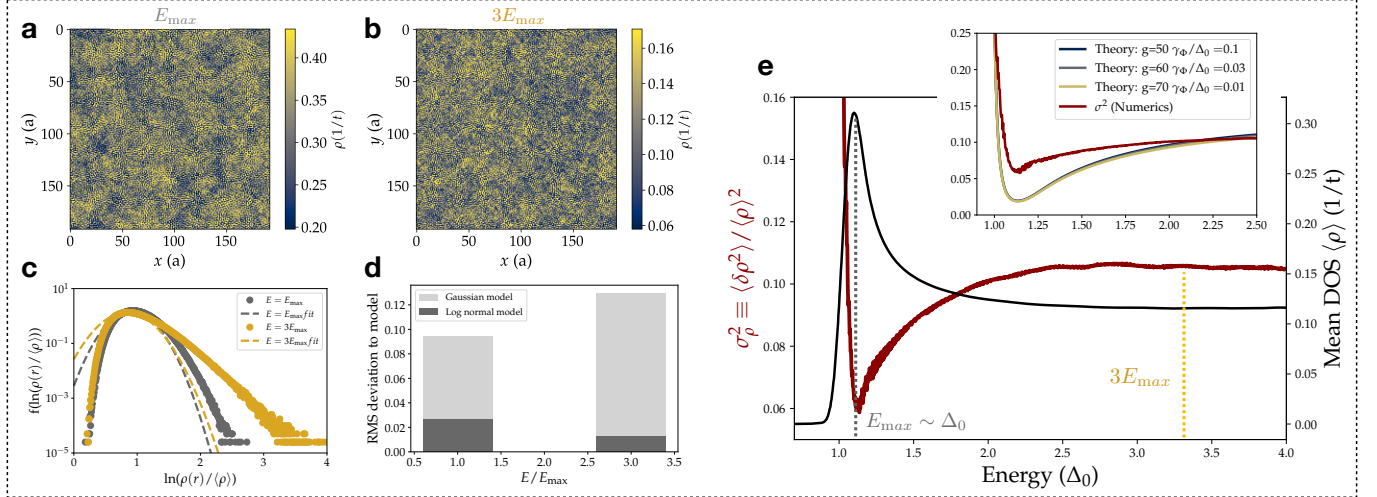
On panels **f-h**, we plot the experimental  $dI/dV$  distribution with gaussian fits (dotted line on **f**). On **g**, the data is given with dots while the dotted line is a gaussian fit and the solid one is a log-normal fit. We stress that the two colors correspond here again to  $E_{\max}$  (grey) and  $3 E_{\max}$  (yellow). Finally, on panel **h**, we show the RMS deviation to gaussian (dotted line) or log-normal (solid line) model. The log-normal model being more accurate is a hint of the multifractal nature of the LDOS fluctuations.

## CONCLUSION

As a model system for a two-dimensional weakly disordered metal, we prepared a single monolayer of lead on silicon where electrons are confined vertically at the Fermi wavelength scale in a controlled crystalline disorder. We report the measurement of tunneling conductance fluctuations with exquisite spatial and spectral resolutions on scales exceeding the superconducting coherence length. Fluctuations are shown to be consistent with the mesoscopic fluctuations physics in the weakly localized regime usually probed through transport measurements. Our measurements yield the energy dependency of these fluctuations close to the superconducting coherence peak and allow to probe their rich spatial structure as a function of energy. The single-point variance spectrum is reproduced semi-quantitatively from first principles without any fitting parameters. The fluctuation's amplitude depends on two parameters which can be probed in this way: the metal's conductance and an effective dephasing rate.

- 
- [1] A. Richardella, P. Roushan, S. Mack, B. Zhou, D. A. Huse, D. D. Awschalom, and A. Yazdani, Visualizing critical correlations near the metal-insulator transition in `ga1-xMnxAs_supp_mat`, *Science* **327**, 665.
  - [2] B. Jäck, F. Zinser, E. J. König, S. N. P. Wissing, A. B. Schmidt, M. Donath, K. Kern, and C. R. Ast, Visualizing the multifractal wave functions of a disordered two-dimensional electron gas, *Physical Review Research* **3**, 013022.
  - [3] K. Zhao, H. Lin, X. Xiao, W. Huang, W. Yao, M. Yan, Y. Xing, Q. Zhang, Z.-X. Li, S. Hoshino, J. Wang, S. Zhou, L. Gu, M. S. Bahramy, H. Yao, N. Nagaosa, Q.-K. Xue, K. T. Law, X. Chen, and S.-H. Ji, Disorder-induced multifractal superconductivity in monolayer niobium dichalcogenides, *Nature Physics* **15**, 904.
  - [4] B. Sacépé, Quantum breakdown of superconductivity in low-dimensional materials, *Nature Physics* **16**, 13.
  - [5] I. S. Burmistrov, I. V. Gornyi, and A. D. Mirlin, Superconductor-insulator transitions: Phase diagram and magnetoresistance, *Physical Review B* **92**, 014506 ().
  - [6] I. S. Burmistrov, I. V. Gornyi, and A. D. Mirlin, Enhancement of the critical temperature of superconductors by anderson localization, *Physical Review Letters* **108**, 017002 ().
  - [7] M. Stosiek, B. Lang, and F. Evers, Self-consistent-field ensembles of disordered hamiltonians: Efficient solver and application to superconducting films, *Physical Review B* **101**, 144503 ().
  - [8] M. Stosiek, F. Evers, and I. S. Burmistrov, Multifractal correlations of the local density of states in dirty superconducting films, *arXiv:2107.06728 [cond-mat]* (), 2107.06728.
  - [9] V. Cherkez, J. Cuevas, C. Brun, T. Cren, G. Ménard, F. Debontridder, V. Stolyarov, and D. Roditchev, Proximity effect between two superconductors spatially resolved by scanning tunneling spectroscopy, *Physical Review X* **4**, 011033.
  - [10] C. Brun, T. Cren, V. Cherkez, F. Debontridder, S. Pons, D. Fokin, M. C. Tringides, S. Bozhko, L. B. Ioffe, B. L. Altshuler, and D. Roditchev, Remarkable effects\_supp\_matt of disorder on superconductivity of single atomic layers of lead on silicon, *Nature Physics* **10**, 444 ().
  - [11] C. Brun, T. Cren, and D. Roditchev, Review of 2d superconductivity: the ultimate case of epitaxial monolayers, *Superconductor Science and Technology* **30**, 013003 ().

Numerics : LDOS fluctuations in attractive Hubbard model



Experiment : LDOS distribution

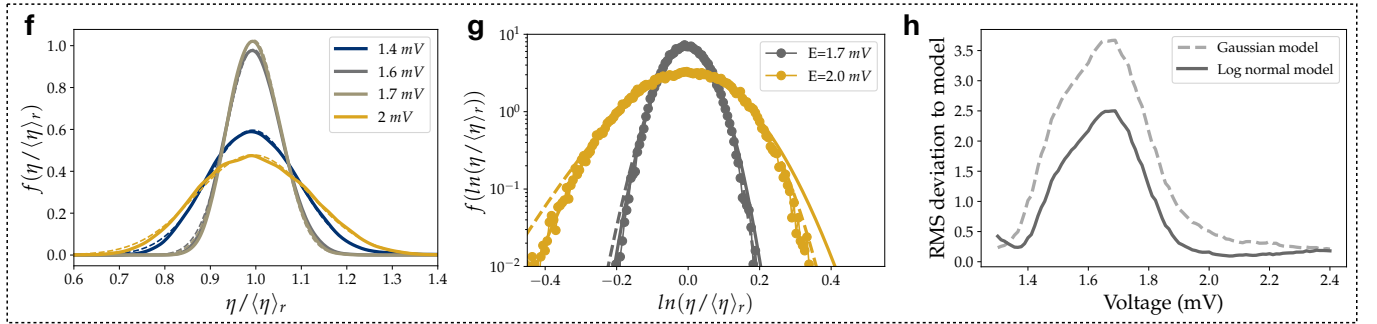


FIG. 5. On panels **a,b**, we show local density of state maps taken at  $E = E_{\max}$  and  $E = 3 E_{\max}$ . On **c**, we plot the LDOS distribution at fixed energy along with the corresponding gaussian fit. On **e**, we show the mean density of states of the numerical model (black line) along with the normalized variance  $\sigma^2$  (red). In the inset, we show a fit to the analytical formula for density of state variance. We show that several values of  $(g, \gamma_\Phi)$  with  $g \in [50, 60, 70]$  allow to reproduce very decently the data. On panels **f-h**, we plot the experimental  $dI/dV$  distribution with gaussian fits (dotted line on **f**). On **g**, the data is given with dots while the dotted line is a gaussian fit and the solid one is a log-normal fit. On **h**, we show the RMS deviation to gaussian (dotted line) or log-normal (solid line) model.